*Khalissa Saada*[1,2], *Salah Amroune*[1,2*], *Moussa Zaoui*[1,2], *Amin Houari*[3], *Kouider Madani*[3], *Mokhtar Benarioua*[4], *Riyadh Benyettou*[1,2]

# NUMERICAL ANALYSIS OF THE MECHANICAL PROPERTIES OF BIOCOMPOSITES IN DIFFERENT GEOMETRIC FORMS

# NUMERIČKA ANALIZA MEHANIČKIH OSOBINA BIOKOMPOZITA ZA RAZLIČITE GEOMETRIJSKE OBLIKE

Originalni naučni rad / Original scientific paper
Rad primljen / Paper received: 1.06.2024
https://doi.org/10.69644/ivk-2025-01-0066

Adresa autora / Author's address:
[1)] Department of Mechanical Engineering, University of Mohamed Boudiaf-M'Sila, Algeria, K. Saada https://orcid.org/0000-0002-3025-1287 ; S. Amroune https://orcid.org/0000-0002-9565-1935
[*]email: salah.amroune@univ-msila.dz ; R. Benyettou https://orcid.org/0000-0002-0095-9524
[2)] Laboratoire de Matériaux, et Mécanique des Structures (LMMS), Université de M'sila. Algérie
[3)] Laboratoire de Matériaux, et Mécanique des Structures (LMMS), Université SBA. Sidi Bel Abesse, Algérie
A. Houari https://orcid.org/0009-0004-2617-2182 ;
K. Madani https://orcid.org/0000-0003-3277-1187
[4)] Mechanical Structures and materials Laboratory, Batna 2, Algeria M. Benarioua https://orcid.org/0009-0000-7383-2017

**Keywords**
- honeycomb
- RE-entrant
- starfish
- load-displacement
- finite element analysis
- biocomposites

**Ključne reči**
- saćasta
- ponovljeni unos reverznim inženjerstvom
- zvezdasti oblik
- opterećenje-pomeranje
- analiza konačnim elementima
- biokompoziti

*Abstract*

*Insulated panels play a crucial role due to their ability to offer a lightweight and cost-effective solution for various applications across different fields, characterised by diverse geometries. In this investigation, three distinct honeycomb shapes - hexagonal, RE-entrant, and starfish - each measuring 57 mm × 120 mm with a thickness of 10 mm, are selected. Epoxy compounds reinforced with date palm, jute, and luffa fibres are utilised in the study. The design of these honeycomb structures was executed using CATIA V5R20® software, while their load-bearing capacity (under compression) was numerically analysed using the ABAQUS-CAE® calculation code. A comparative numerical analysis was conducted to evaluate the performance of the samples based on the different types of honeycombs employed. Following compression tests conducted at a rate of 0.2 mm/min, the findings revealed that the starfish structure exhibited the highest pressure-carrying capacity. Specifically, it sustained loads of 2220.75 N for the epoxy sample, 3107.74 N for the date palm fibre samples, and 3352.20 N for sisal fibre samples. Notably, the sisal fibre sample demonstrated the highest strength, 4338.33 N, while comparatively lower strength values were observed for RE-entrant geometries, particularly for the honeycomb reinforced with date palm fibres.*

*Izvod*

*Izolovani paneli imaju važnu ulogu zbog svojih karakteristika male težine i isplativih rešenja kod raznih primena u mnogim oblastima, sa širokim rasponom geometrijskih oblika. U ovom istraživanju bavimo se različitim saćastim oblicima konstrukcija - heksagonalna, reverzno-inženjerska ulazna (RE-entrant) i zvezdasta - svaka sa dimenzijama 57 mm × 120 mm i debljine 10 mm. Upotrebljeni su materijali tipa epoksi jedinjenja ojačana urminom palmom, jutom i vlaknima lufe. Proračun ovih saćastih konstrukcija je izveden primenom softvera CATIA V5R20®, a kapacitet nosivosti (u uslovima pritiska) je numerički analiziran primenom alata za proračun ABAQUS-CAE®. Izvedena je uporedna numerička analiza za procenu performansi uzoraka, na bazi različitih upotrebljenih saćastih modela. Na osnovu ispitivanja pritiskom izvedenih pri brzini 0,2 mm/min, rezultati pokazuju da najveći kapacitet nosivosti pod pritiskom ima zvezdasta konstrukcija. Zapravo, u slučaju epoksi uzorka, može da nosi opterećenje od 2220,75 N, 3107,74 N za uzorak sa vlaknima od urma palme, 3352,20 N za uzorak od vlakana agave. Uzorak od vlakana agave pokazao je najveću čvrstoću, 4338,33 N, dok su manje vrednosti čvrstoće imale geometrije tipa RE-entrant, posebno u slučaju saćaste konstrukcije ojačane vlaknima urmine palme.*

## INTRODUCTION

Honeycomb structures come in a wide variety of geometric configurations, with the hexagonal shape being the most common /1-3/. Over the past decade, the naval and aerospace industries have widely adopted these structures - made from various materials - for the fabrication of sandwich panels. The hexagonal configuration is particularly valued for its lightness and low cost, /4/. Moreover, honeycomb structures are also used in other fields such as automotive, civil aviation, and transportation /5-7/. In addition to the hexagonal form, other variants exist, including circular structures /8/, re-entrant structures /9-11/, combinations of hexagonal and re-entrant designs /12-14/, triangular and other specific models /15/, as well as starfish-shaped structures /16/.

Several studies have focused on characterising honeycomb structures both numerically and experimentally to achieve mechanical properties such as traction, compression and torsion. For example, Krishna et al. /2/ used the hexagonal titanium and aluminium honeycomb structure for bending tests on an ANSYS® calculation code. The authors concluded that the titanium structure is better than the aluminium one, but expensive and heavier. Tabacu and Ducu /17/ formed a compression test on a set of structures, including a hive, lattice, honeycomb, and a rectangular structure. Both researchers noted that there was convergence between experimental and numerical results. Ghongade et al. /18/ studied honeycombs with a circular structure (with and without reinforcement) in which a set of steel tubes were welded. A numerical analysis of compression loads was performed using ABAQUS® software and it was found that reinforced honeycombs had the highest bearing capacity. Xia et al. /19/ studied three aluminium alloy structures inspired by a honeycomb. The authors applied axial compression to the samples to measure energy absorption, in the same way Xu et al. /20/ made honeycomb (RE-entrant) samples filled with aluminium foam and noticed that aluminium foam increased energy absorption resistance due to its compressive strength. Ganesh et al. /21/ performed bending tests on hexagonal honeycomb structures made of aluminium, titanium, and steel using CATIA® and ANSYS® software. They noted that aluminium and titanium have higher bending strength than steel, but titanium is also heavier.

In this article, we study three different types of honeycombs made from epoxy biocomposites reinforced with date palm, jute, and luffa fibres (hexagonal, RE-entrant, and starfish). Samples are designed using CATIA® software. Additionally, the ABAQUS® programme is used to determine and improve their mechanical properties. We have conducted pressure testing on the specimens. Finally, we compare the results of samples with different structures to understand the geometric effect of honeycombs on their mechanical properties. The aim of this study is to choose the best composition among the three proposed geometric shapes in terms of mechanical properties for later use in mechanical applications and structures.

## THEORETICAL FRAMEWORK

Honeycombs studied in this article are subjected to a force $F$, which can be tensile or compressive. The force along the $S$ section can be calculated using the following equation /22, 23/:

$$F_s = \int_{dS} \sigma dS\,, \quad F_e = \sigma_e S_e \text{ (inelastic level)},$$

$$F_e = E_e \varepsilon_e S_e \text{ (elastic level)},$$

$$\sigma = \frac{f_s}{1.5}\left(1-\left(1-\frac{\varepsilon}{0.02}\right)^2\right)0.85\,\cdot$$

Then, the quasi-static stress of the tray $\sigma$ in the auxetic honeycomb is given by /24/:

$$\sigma = \frac{\int_0^N \sigma(\varepsilon)d\varepsilon}{N}\,,$$

where: $\varepsilon$ and $\sigma(\varepsilon)$ are the compressive strain and crushing stress, respectively; and $N$ is densification strain.

The Jones-Wilkens-Lee equation is used to calculate the pressure generated as shown in Eq.(1) /25/:

$$P = b_1\left(1-\frac{\eta}{C_1 V}\right)e^{-CV} + b_2\left(1-\frac{\eta}{C_2 V}\right)e^{-CV} + \left(\frac{\eta E}{V}\right),$$

where: $V$ is relative volume of the explosive product; $E$ is the internal energy per unit volume; $b_1$, $b_2$, $C_1$, $C_2$, $\eta$ are empirical constant derivatives for explosives (ABAQUS/CAE).

The method was used to measure stress. The Poisson coefficient of the sample can be calculated from the longitudinal elongation, according to the formula /14/:

$$\nu_{jk} = -\frac{\varepsilon^y_{jk}}{\varepsilon^z_{jk}} = -\frac{\Delta^y_{jk}}{\Delta^z_{jk}}\frac{A_z}{A_y} = -\frac{[Y_{j(k+1)} - Y_{j(k-1)}]}{[Z_{k(j+1)} - Z_{k(j-1)}]}\frac{A_z}{A_y}\,,$$

$$(2 \le j \le 3,\ 2 \le k \le 3)\,,\quad \bar{\nu} = \frac{1}{4}\sum \nu_{jk}\,,$$

where: $\nu_{jk}$ is Poisson coefficient; $A_Z$, $\Delta^y$ are respectively the horizontal and vertical distances of consecutive points of undeformed specimens; $\varepsilon_{jk}^y$ transverse deformation; $\varepsilon_{jk}^z$ axial deformation; $Y$, $Z$ are real-time coordinates of points.

The Hu-Washizu form of the mechanical problem is defined by the minimisation problem of functional. The solid deforms under the effect of density forces $f_v$, it is subject to forces $t_N$ imposed on $\partial_N S_0$ /26/,

$$k(u,H,P) = \int_{S_0} \psi_{mec}(F) + (\nabla_x u - H) : \int_{S_0} f_V u - \int_{\partial_N S_0} t_N u\,,$$

where: $u$ is displacement, $\nabla_x$ is the gradient of displacement field; $P$ is first Piola-Kirchoff tensor; $\psi_{mec}$ denotes the mechanical energy potential of the system and the gradient of the transformation.

## GEOMETRY OF MICROSTRUCTURES AND REPRESENTATIVE VOLUME ELEMENT

There are many types of artificial honeycombs. In this study, we chose to work with three types of honeycomb structures (hexagonal, RE-entrant, and starfish) which have also been used in other research, as in /12, 27, 28/. As shown in Fig. 1, the starfish structure has 30 cells of size 121 mm × 57 mm × 10 mm, resulting from a number of cells 3 × 4 (width × height). The honeycomb structures are designed using CATIA® software with dimensions 127×20×10 mm$^3$ for each cell unit manufactured with dimensions 18 × 21 × 10 mm$^3$. The different dimensions of the honeycombs used are presented in Table 1. The designed honeycombs are then digitally analysed using ABAQUS® software.

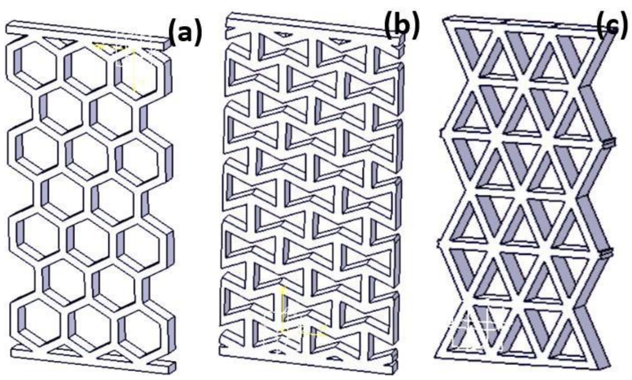


Figure 1. Microstructure textures at different scales: a) hexagonal, b) RE- entrant c) star-fish.

## MATERIALS AND METHODS

After the 3D-printed honeycomb samples (honeycomb, starfish, RE-entrant) were prepared on a 3D printer, they are carefully placed within a wooden mould and securely fixed to prevent any movement during the silicone pouring process, as shown in Fig. 2. Subsequently, the stage of pouring liquid silicone into the wooden mould, housing the beehive samples, ensued. To ensure a level surface for the mould containing the 3D-printed samples, a level tool is employed. Liquid silicone is then poured slowly into the mould until the samples are submerged 3 mm. At this point, the pouring of silicone liquid ceased, as depicted in Fig. 3. To mitigate the risk of air and bubbles getting trapped in the mould, it is advisable to expel the gas using a hairdryer, elevating any trapped bubbles within the mould.

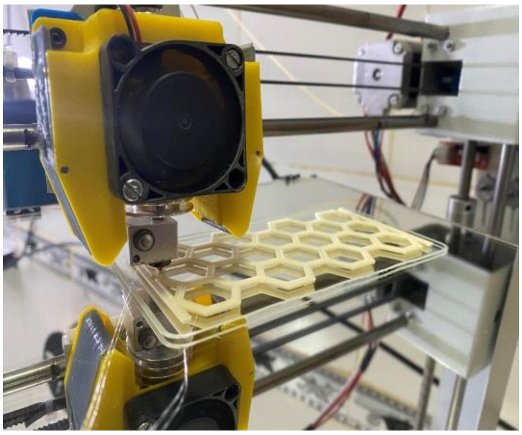

Figure 2. Three-dimensional printer used for our work.

Figure 3. Positioned printed samples securely within a wooden mould.

Biocomposites of honeycomb samples (hexagonal, RE-entrant, and starfish) are manufactured using a moulding process in pre-made silicone moulds, following the steps:

1. Fibre preparation: palm, jute, and luffa fibres are obtained and cut into small 1 mm pieces. The fibre content was set at 20 % for each type, in accordance with prior research /29/.
2. Mixing: the cut fibres are combined with epoxy resin at a ratio of 3.75 grams of resin to 1.25 grams of hardener. The mixture is thoroughly mixed with a plastic spoon to ensure homogeneity.
3. Moulding: the homogeneous mixture is then poured into silicone moulds, creating pressure specimens corresponding to hexagonal, RE-entrant, and starfish designs.
4. Drying: specimens were allowed to dry for 24 hours at room temperature.
5. Electrophoresis: subsequently, specimens are transferred to an electrophoresis oven to facilitate the crystallisation of the resin. The temperature is maintained at 60 °C for 5 hours.

The entire process is illustrated in Figs. 4 and 5.

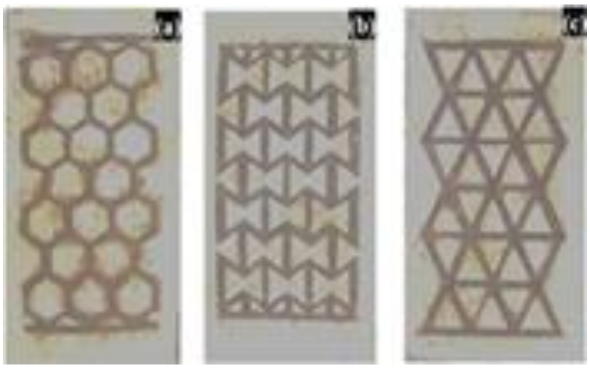


Figure 4. Moulding biocomposite samples in a silicone mould: a) hexagonal; b) RE-entrant; and c) starfish.

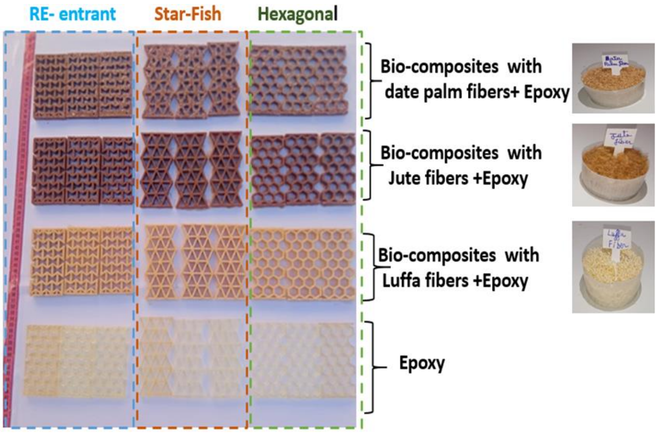


Figure 5. Honeycomb samples of biocomposites.

## EXPERIMENTAL ANALYSIS

The objective of this section is to assess the performance of the beehive biocomposite reinforced with different fibre tissues (sisal, luffa, date palm, and epoxy). Epoxy samples are included as controls and subjected to a compression test with a transmission speed of 0.2 mm/min.

Figure 6 illustrates results of compression tests conducted on honeycomb samples with various geometries, including hexagonal, RE-entrant, and starfish, each integrated with different bio composites with a fibre ratio of 20. The graphical representation reveals the mechanical properties of each type of biocomposites. The average encapsulated force results for all samples under compression are depicted.

Among the tested compounds, luffa fabric compounds (luffa biocomplex) exhibited the highest force values, measuring 868.04 ± 87.27 N. For hexagonal honeycomb engineering, the force was 245.39 ± 20.07 N, while for RE-entrant honeycomb engineering, it was 2975.49 ± 188.96 N. In the case of starfish honeycomb engineering, the force was shown to be considerably higher.

As depicted in Figs. 5a, 5b, and 5c, the texture compounds for bees in engineering showed honeycomb structures resembling star-fish, demonstrating significantly greater force values compared to hexagonal and RE-entrant forms.

In Fig. 7, experimental results are presented for the honeycomb in three different geometries: hexagonal, RE-entrant, and starfish, using fibre-reinforced epoxy compounds such as sisal, luffa, and date palm. The curves representing average values for these three samples (hexagonal, RE-entrant, and starfish) are depicted, showcasing the results of compression tests for force and transmission.

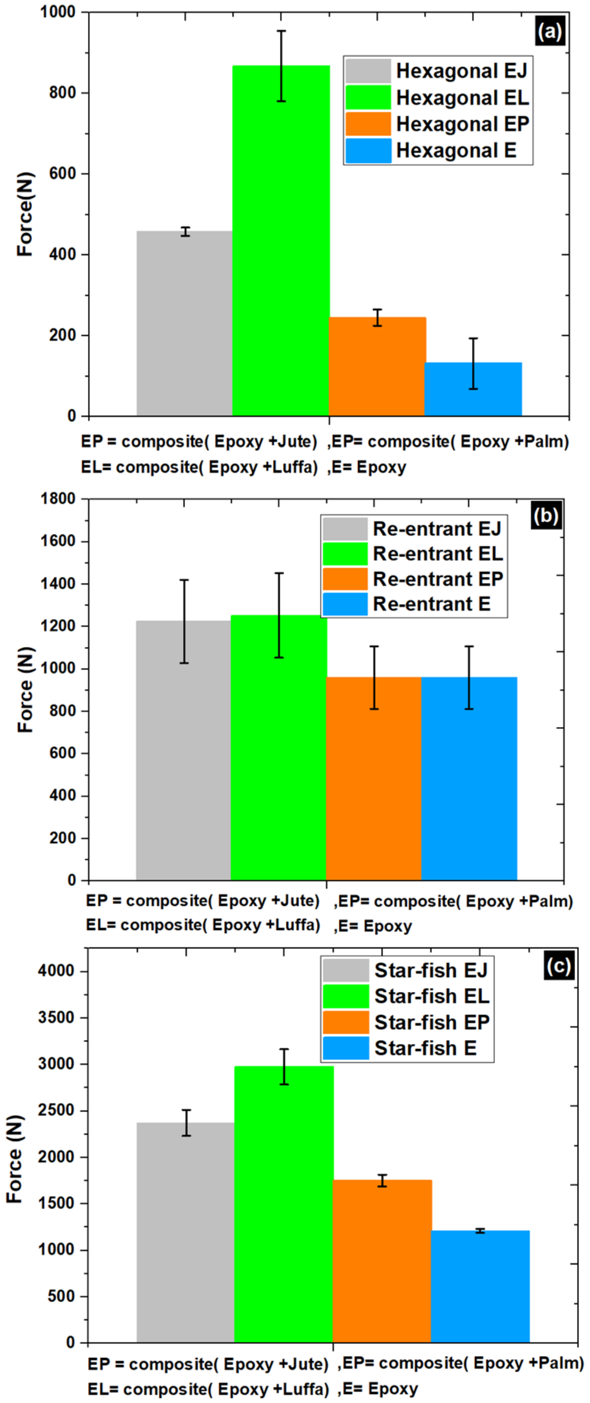


Figure 6. Evolution of mechanical properties of bio-composites for force: a) hexagonal; b) RE-entrant; and c) starfish.

The outcomes highlight the influence of honeycomb varying geometry on mechanical properties during compression tests. Notably, maximal strength values are observed for the star-fish sample, 2220.75 N for the epoxy sample, 3107.74 N for date palm fibre samples, and 3352.20 N for sisal fibre samples. The luffa fibre sample exhibited the highest force value at 4338.33 N, while lower force values are recorded for hexagonal and RE-entrant geometries, particularly for honeycomb with date palm fibres.

In the case of the RE-entrant shape, the highest force value was 989.19 N for the epoxy sample, 1016.89 N for date palm fibre samples, and 1171.35 N for sisal fibre samples. The luffa fibre sample again showed the highest force value at 1327.47 N. For the hexagonal honeycomb geometry, the force values were 219.33 N for epoxy sample, 550.32 N for date palm fibre samples, and 893.87 N for sisal fibre samples. The highest force value recorded was 951.27 N for the luffa fibre sample, aligning with findings from previous research.

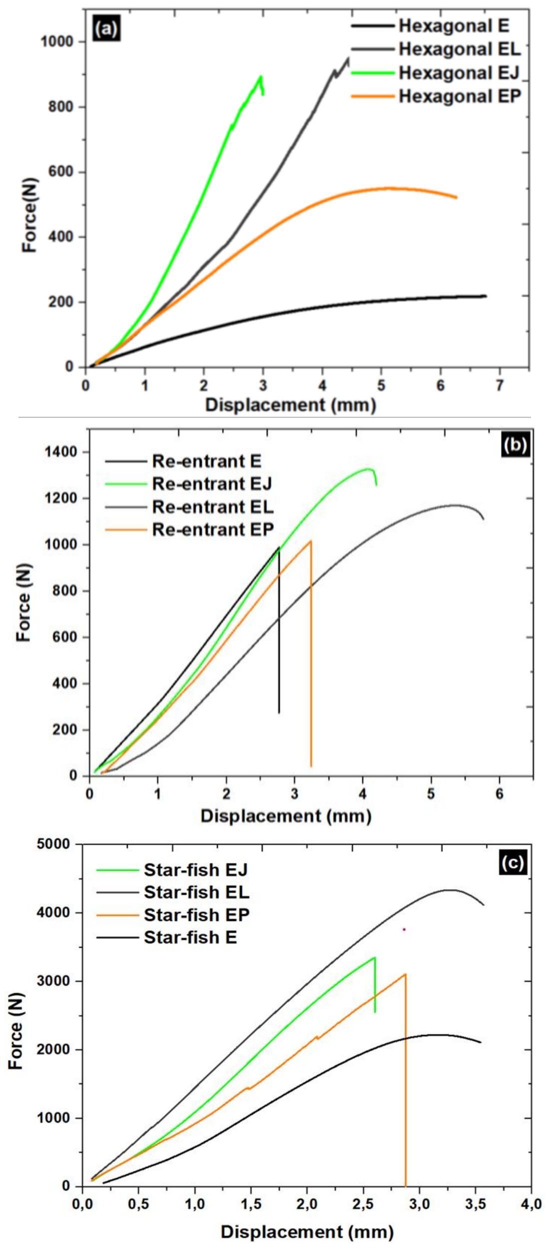


Figure 7. Force-displacement for bio-composite: a) hexagonal; b) RE-entrant; and c) starfish.

## NUMERICAL ANALYSIS

### *Finite element modelling (FE)*

This analysis is performed digitally using general purpose finite element software ABAQUS® v16.14. The mesh layout is used for each type of honeycomb (hexagonal, RE-entrant, and starfish) using 3D continuum hexahedral elements (type ABAQUS C3D8R) for all volumes from 57×120×10 mm$^3$, indicating the autonomy of the models. Finally, a mesh grid of overall size of about 1 mm is chosen for the division of each element, giving 29,840 nodes and 37,570 elements. The results of this analysis are presented in Table 1.

Table 1 . Input parameters in the mesh part.

| Type of honeycomb | Type of mesh | Approximate global size | Number of nodes | Number of elements |
|---|---|---|---|---|
| Hexagonal | continuum-3D hexagonal C3D8R | 1 | 29 840 | 37 570 |
| RE-entrant | continuum-3D hexagonal C3D8R | 1 | 29 840 | 37 570 |
| Starfish | continuum-3D hexagonal C3D8R | 1 | 29 840 | 37 570 |

a)

b)

c)

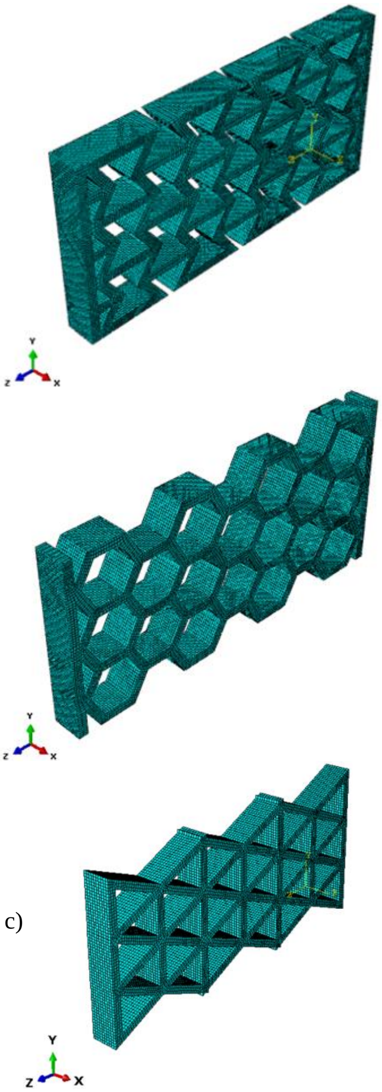

Figure 8. Three models of honeycombs (3D) in structured mesh form: a) RE-entrant; b) hexagonal; c) starfish.

The compression test behaviour of beehive structures investigated in this study is influenced by rupture mechanisms. Unlike stem cell flame-induced unstable rupture observed in some materials, natural fibre/epoxy structures do not exhibit such behaviour. Additionally, they show reduced damage resulting from failure mechanisms commonly observed in fibre composites, such as fibre retreat, fibre rupture, and axial rupture, as illustrated in Fig. 9. On the contrary, the heterogeneity in natural/epoxy composite fibres, arising from local variations in properties and fibre orientation, may act as a preferential site for damage. The damage after breaking occurred within the cell structure of the honeycomb that varied depending on the shape of the honeycomb and the type of fibre used.

Figure 9. Samples of honeycomb after compression test.

## CONCLUSIONS

A detailed analysis and objective comparison of recent studies is conducted on the application of finite element analysis to honeycombs. The ABAQUS/CAE® software is used to study the effect of compression on different types of honeycombs (RE-entrant, hexagonal, and starfish). By comparing the simulation results, we come to the following conclusions:

- loads induce a more localised deformation in the structure which can lead to an early onset of plasticity and localised instability;
- the honeycomb cell with starfish geometry is more suitable to withstand loads such as tension and compression compared to the hexagonal honeycomb cell and the RE-entrant cell. The maximal load was reached for the starfish sample, reaching 2220.75 N for epoxy sample, 3107.74 N for date palm fibre samples, and 3352.20 N for sisal fibre samples;
- finally, the honeycomb structure with RE-entrant geometry has the best impact resistance during axial impacts (compression). This type of structure can be made of biocomposites and is used in the equipment of some aircraft, as well as in product packaging.

## REFERENCES

1. Khan, M.S., Abdul-Latif, A., Koloor, S.S.R., et al. (2021), *Representative cell analysis for damage-based failure model of polymer hexagonal honeycomb structure under the out-of-plane loadings*, Polymers, 13(1): 52. doi: 10.3390/polym13010052

2. Audibert, C., Andréani, A.-S., Lainé, É., Grandidier, J.-C. (2019), *Discrete modelling of low-velocity impact on Nomex® honeycomb sandwich structures with CFRP skins*, Compos. Struct. 207: 108-118. doi: 10.1016/j.compstruct.2018.09.047
3. Li, J., Liu, J., Liu, H., Yang, J. (2020), *A precise theoretical model for laterally crushed hexagonal tubes*, Thin-Walled Struct. 152: 106750. doi: 10.1016/j.tws.2020.106750
4. Chen, X., Yu, G.-C., Wang, Z., et al. (2021), *Enhancing out-of-plane compressive performance of carbon fiber composite honeycombs*, Compos. Struct. 255: 112984. doi: 10.1016/j.compstruct.2020.112984
5. Krishna, P.S., Vemula, A.M., Ahamed, P.U., Jani, S.P. (2022), *Bending analysis of honeycomb sandwich panels with metallic face sheets and GFRP core*, Mater. Today: Proc. 60(Part 3): 1537-1547. doi: 10.1016/j.matpr.2021.12.050
6. Rekbi, F.M.L., Hecini, M., Khechai, A. (2018), *Experimental and numerical analysis of mode-I interlaminar fracture of composite pipes*, J Braz. Soc. Mech. Sci. Eng. 40(10): 502. doi: 10.1007/s40430-018-1423-y
7. Khechai, A., Belarbi, M.-O., Bouaziz, A., Rekbi, F.M.L. (2022), *A general analytical solution of stresses around circular holes in functionally graded plates under various in-plane loading conditions*, Acta Mechanica, 234(1): 1-21. doi: 10.1007/s00707-022-03413-1
8. Tang, H.P., Wang, Q., Yang, G.Y., et al. (2016), *A honeycomb-structured Ti-6Al-4V oil-gas separation rotor additively manufactured by selective electron beam melting for aero-engine applications*, JOM, 68(3): 799-805. doi: 10.1007/s11837-015-1778-9
9. Indreș, A.I., Constantinescu, D.M., Mocian, O.A. (2021), *Bending behavior of 3D printed sandwich beams with different core topologies*, Mater. Des. Proces. Comm. 3(10): e252. doi: 10.1002/mdp2.252
10. Shao, Y., Meng, J., Ma, G., et al. (2021), *Insight into the negative Poisson's ratio effect of the gradient auxetic reentrant honeycombs*, Comp. Struct. 274(17): 114366. doi: 10.1016/j.compstruct.2021.114366
11. Yu, R., Luo, W., Yuan, H., et al. (2020), *Experimental and numerical research on foam filled re-entrant cellular structure with negative Poisson's ratio*, Thin-Walled Struct. 153(9): 106679. doi: 10.1016/j.tws.2020.106679
12. Geramizadeh, H., Dariushi, S., Salami, S.J. (2022), *Optimal face sheet thickness of 3D printed polymeric hexagonal and re-entrant honeycomb sandwich beams subjected to three-point bending*, Compos. Struct. 291: 115618. doi: 10.1016/j.compstruct.2022.115618
13. Namvar, N., Zolfagharian, A., Vakili-Tahami, F., Bodaghi, M. (2022), *Reversible energy absorption of elasto-plastic auxetic, hexagonal, and AuxHex structures fabricated by FDM 4D printing*, Smart Mater. Struct. 31(5): 055021. doi: 10.1088/1361-665X/ac6291
14. Luo, H.C., Ren, X., Zhang, Y., et al. (2022), *Mechanical properties of foam-filled hexagonal and re-entrant honeycombs under uniaxial compression*, Compos. Struct. 280: 114922. doi: 10.1016/j.compstruct.2021.114922
15. Habib, F.N., Iovenitti, P., Masood, S.H., Nikzad, M. (2018), *Cell geometry effect on in-plane energy absorption of periodic honeycomb structures*, Int. J Adv. Manuf. Technol. 94(5): 2369-2380. doi: 10.1007/s00170-017-1037-z
16. Saufi, S.A.S.A., Zuhri, M.Y.M., Dezaki, M.L., et al. (2021), *Compression behaviour of bio-inspired honeycomb reinforced starfish shape structures using 3D printing technology*, Polymers, 13(24): 4388. doi: 10.3390/polym13244388
17. Tabacu, S., Ducu, C.M. (2020), *Numerical investigations of 3D printed structures under compressive loads using damage and fracture criterion: Experiments, parameter identification, and validation*, Extreme Mech. Let. 39: 100775. doi: 10.1016/j.eml.2020.100775
18. Ghongade, G., Kalyan, K.P., Vignesh, R.V., Govindaraju, M. (2021), *Design, fabrication, and analysis of cost effective steel honeycomb structures*, Mater. Today: Proc. 46(Part 10): 4520-4526. doi: 10.1016/j.matpr.2020.09.694
19. Xia, H., Sun, Q., Wang, S. (2023), *Influence of strain rate effect on energy absorption characteristics of bio-inspired honeycomb column thin-walled structure under impact loading*, Case Stud. Constr. Mater. 18: e01761. doi: 10.1016/j.cscm.2022.e01761
20. Xu, H.H., Luo, H.C., Zhang, X.G., et al. (2023), *Mechanical properties of aluminum foam filled re-entrant honeycomb with uniform and gradient designs*, Int. J Mech. Sci. 244: 108075. doi: 10.1016/j.ijmecsci.2022.108075
21. Ganesh, B., Kumar, B.V., Muppala, D. (2015), *Design and structural analysis of aircraft floor panel*, Int. J Adv. Eng. Global Technol. 3(12): 1451-1460.
22. Caycedo Garcia, M.S., Siqueira, G.H., Vieira Junior, L.C.M., Vizotto, I. (2019), *Evaluation of structural capacity of triangular and hexagonal reinforced concrete free-form shells*, Eng. Struct. 188: 519-537. doi: 10.1016/j.engstruct.2019.03.044
23. Saada, K., Amroune, S., Zaoui, M., et al. (2023), *Experimental and numerical study of the effect of the presence of a geometric discontinuity of variable shape on the tensile strength of an epoxy polymer*, Acta Mechanica et Automatica, 17(2): 192-199. doi: 10.2478/ama-2023-0022
24. Dong, Z., Li, Y., Zhao, T., et al. (2019), *Experimental and numerical studies on the compressive mechanical properties of the metallic auxetic reentrant honeycomb*, Mater. Des. 182: 108036. doi: 10.1016/j.matdes.2019.108036
25. Keskin, İ., Yadgar Ahmed, M., Ramadhan Taher, N., et al. (2022), *An evaluation on effects of surface explosion on underground tunnel; availability of ABAQUS Finite element method*, Tunnel. Undergr. Space Technol. 120: 104306. doi: 10.1016/j.tust.2021.104306
26. Siedel, D., Helfer, T., Fandeur, O., et al. (2022), *Schéma de résolution locale pour la méthode Hybrid High Order et application en mécanique non-linéaire (Local resolution scheme for the Hybrid High Order method and its application in nonlinear mechanics)*, In : 15th National Conf. on Structural Computations, May 2022, Giens (Var), France. (in French)
27. Hosseinabadi, H.G., Bagheri, R., Gray, L.A., et al. (2017), *Plasticity in polymeric honeycombs made by photo-polymerization and nozzle based 3D-printing*, Polymer Test. 63: 163-167. doi: 10.1016/j.polymertesting.2017.08.008
28. Colatosti, M., Fantuzzi, N., Trovalusci, P., Masiani, R. (2022), *New insights on homogenization for hexagonal-shaped composites as Cosserat continua*, Meccanica, 57(4): 885-904. doi: 10.1007/s11012-021-01355-x
29. Saada, K., Zaoui, M., Amroune, S., et al. (2023), *Exploring tensile properties of bio composites reinforced date palm fibers using experimental and modelling approaches*, Mater. Chem. Phys. 314: 128810. doi: 10.1016/j.matchemphys.2023.128810